High Energy Physics and Nuclear Physics
Volume 17, Number 2

Effect of Interaction Range in Relativistic Microscopic Optical Potential

Zhu Ping, Xu Jiabao and Gao Qin

(Department of Physics, Hangzhou University, Zhejiang, China)

In the Walecka model of the relativistic nucleon-meson field theory, by using the models nucleon-nucleon interaction, the optical potential (OP) in the local density approximation (LDA) is folded, so that the effect of the interaction range on the relativistic nucleon-nucleus microscopic optical potential can be discussed. With this OP, the differential cross section of the nuclear elastic scattering and spin observables are analyzed. Comparing with the result calculated in LDA, a better agreement between our result and the experimental data is obtained.

1. INTRODUCTION

In recent years, increased attention has been paid to the investigation of the relativistic optical potential [1-8]. One method of studying the relativistic microscopic optical potential (RMOP) can be briefly illustrated in the following. Based on the Walecka model of the relativistic nucleon-meson field theory [9], OP can be calculated in the lowest-order approximation. Namely, the Hartree-Fock self-energy is taken as the real part of OP and the imaginary part of the self-energy from the polarization diagram is considered as the imaginary part of OP. For a finite nucleus, OP is usually evaluated in LDA. In terms of this potential, the nucleon-nucleus elastic scattering can be studied and the satisfactory result can be obtained. However, in LDA the effect of nucleon-nucleon interaction range on the finite nucleus is ignored. By comparing this finite-nucleus OP and the phenomenological

Received on January 9, 1991. Supported by the National Natural Science Foundation of Zhejiang, China. © 1994 by Allerton Press, Inc. Authorization to photocopy individual items for internal or personal use, or the internal or personal use of specific clients, is granted by Allerton Press, Inc. for libraries and other users registered with the Copyright Clearance Center (CCC) Transactional Reporting Service, provided that the base fee of $50.00 per copy is paid directly to CCC, 27 Congress St., Salem, MA 01970. An annual license may be obtained only directly from Allerton Press, Inc. 150 5th Avenue, New York, NY 10011.

potential, it is found that they differs to a certain extent on the nuclear surface, and the root mean square radius of OP, as an important physical quantity to characterize OP, is generally smaller in the LDA case than in the phenomenological case. In this investigation, by employing the nucleon-nucleon interaction obtained from the Walecka model, the OP is folded in LDA, the effect of the interaction range of the nuclear force on the nucleon-nucleus microscopic OP is studied and consequently, the LDA calculation is improved. In Sec.2, the folding method is illustrated, and the result and discussion are given in Sec.3.

2. FORMALISM

In the Walecka model, the Lagrangian density [9] of the nucleon who interacts with each other via σ-and ω-meson exchanges is written as

$$\begin{aligned}\mathscr{L} = & \bar{\Psi}(i\gamma^{\mu}\partial_{\mu} - M)\Psi + \frac{1}{2}(\partial^{\mu}\partial_{\mu}\sigma - m_{\sigma}^{2}\sigma^{2}) \\ & + \frac{1}{2}m_{\omega}^{2}\omega^{\mu}\omega_{\mu} - \frac{1}{2}F^{\mu\nu}F_{\mu\nu} - g_{\sigma}\bar{\Psi}\sigma\Psi \\ & - g_{\omega}\bar{\Psi}\gamma^{\mu}\omega_{\mu}\Psi\end{aligned} \tag{1}$$

where $F_{\mu\nu} = \partial_{\mu}\omega_{\nu} - \partial_{\nu}\omega_{\mu}$, Ψ, σ, and ω_{μ} are the nucleon, σ-meson and ω-meson field operators, respectively, and M, m_{σ} and m_{ω} are the masses of the nucleon, σ-meson and ω-meson, with their values $M = 938.9$ MeV, $m_{\sigma} = 550$ MeV, $m_{\omega} = 770$ MeV, respectively. In the Hartree-Fock approach, the coupling constant between the nucleon and meson is determined by fitting the saturated properties of nuclear matter. Here, the Fermi kinetic energy of the saturated nuclear matter is taken as $k_F = 1.42$ fm^{-1}, correspondingly, $g_{\sigma}^{2}/4\pi = 6.63$, and $g_{\omega}^{2}/4\pi = 8.62$.

It is clear that the nucleon self energy in nuclear medium is just the nucleon-nucleus effective interaction, i.e., nucleon-nucleus optical potential. In the lowest approximation, the Hartree-Fock self energy of the nucleon is the real part of OP, and the contributions of polarization diagrams are the imaginary part of OP. In the nuclear matter whose Fermi kinetic energy is k_F (density $\rho = 2/3\pi^2 k_F^3$), the on-shell nucleon OP is[1,2]

$$\begin{aligned}\sum(k_F, E) = & \sum_{s}(k_F, E) - \gamma^{0}\sum_{0}(k_F, E) \\ & + \boldsymbol{r}\cdot\boldsymbol{k}\sum_{v}(k_F, E).\end{aligned} \tag{2}$$

where

$$\sum_{i}(k_F, E) = V_i(k_F, E) + iW_i(k_F, E). \tag{3}$$

with $i = s$, o, and v being the scalar, vector, and three-vector, respectively. V_i and W_i denote the Hartree-Fock self energy and the imaginary part of the self-energies of polarization diagrams. For simplicity, we do not give their explicit expressions [2]. Since the self-consistent calculation of the finite nucleus OP is a rather difficult problem, one usually makes LDA so the OP for a nucleon at a certain point in the finite nucleus equals that in the nuclear matter with corresponding density

$$\sum^{\mathrm{LDA}}(r, E) = \sum(k_F(r), E). \tag{4}$$

Let us choose OP in the Hartree-Fock approximation as a sample to analyze the defect of LDA. In the Hartree approximation, the σ- and ω-meson exchanges cause the scalar potential V_s and vector

potential V_0, respectively. If one substitutes N-N interactions induced by the σ- and ω-meson exchanges by local potentials v_σ and v_ω, respectively, the exact solution of OP for a nucleon in the finite nucleus in the Hartree-approximation is

$$V^{\mathrm{IFN}}(r) = \int \rho_l(r')v_l(r - r')\mathrm{d}r. \tag{5}$$

where $l = \sigma$ and ω, $V^\sigma = V_s$, $V^\omega = V_0$, and ρ_σ and ρ_ρ are the scalar and vector densities, respectively [9]. The OP for a nucleon in nuclear matter reads

$$V^{\mathrm{INM}} = \rho_l \int v_l(r')\mathrm{d}r'. \tag{6}$$

and the corresponding nucleon-nucleus OP in LDA reads

$$V^{\mathrm{ILDA}} = \rho_l(r) \int v_l(r')\mathrm{d}r'. \tag{7}$$

Obviously, only if the interaction range equals zero, Eq.(5) is equivalent to Eq.(7). However, the interaction between nucleons is not a zero-range interaction. Due to the very short-range character of the N-N interaction, LDA is still a more effective approximation. Especially in the center of the nucleus, because the density distribution is almost a constant, LDA is good enough. But at the surface region of the nucleus, this approximation increases, because the nuclear density rapidly decreases there.

To consider the effect of the interaction range in the finite nucleus, one folds V^{ILDA}, OP in LDA, with the N-N interaction $v_l(r-r')$ [10], and obtains the improved OP

$$V^{\mathrm{I}}(r) = C_l \int V^{\mathrm{ILDA}}(r')v_l(r - r')\mathrm{d}r'. \tag{8}$$

where the constant $C_l = [\int v_l(r')\mathrm{d}r']^{-1}$ is chosen according to the fact that $V^{\mathrm{IILDA}} = V^{\mathrm{ILDA}}$ in nuclear matter. It is easy to prove that V^{I} exactly equals to V^{IFN} in the Hartree approximation. Namely, substituting Eq.(7) into Eq.(8), one has

$$\begin{aligned} V^{\mathrm{I}}(r) &= C_l \int \rho(r')v_l(r - r')[\int \mathrm{d}r'' v_l(r'')]\mathrm{d}r' \\ &= \int \rho_l(r')v_l(r - r')\mathrm{d}r'. \end{aligned} \tag{9}$$

Obviously, for the OP in the Hartree approximation, the above method effectively improves the calculation in LDA.

Strictly speaking, in the Walecka model, the interaction between nucleons caused by the meson exchange cannot be expressed by a potential. However, in the non-relativistic limit, due to the large nucleon mass, the interactive cannot be related to the time and spin again. It can be expressed by the Ynkawa potential in coordinate space [9]

$$v_\sigma(r - r') = -\frac{g_\sigma^2}{4\pi} \cdot \frac{\mathrm{e}^{-m_\sigma|r-r'|}}{|r - r'|}, \tag{10a}$$

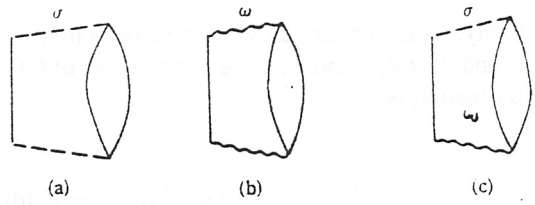

Fig. 1
Polarization diagrams.

$$v_\omega(\boldsymbol{r}-\boldsymbol{r}') = \frac{g_\omega^2}{4\pi}\cdot\frac{e^{-m_\omega|\boldsymbol{r}-\boldsymbol{r}'|}}{|\boldsymbol{r}-\boldsymbol{r}'|}. \tag{10b}$$

By considering the finite size of the nucleon, a cut-off factor Λ_l should be introduced, then the potential can be rewritten as

$$v_\sigma(\boldsymbol{r}-\boldsymbol{r}') = -\frac{g_\sigma^2}{4\pi}\frac{1}{|\boldsymbol{r}-\boldsymbol{r}'|}(e^{-m_\sigma|\boldsymbol{r}-\boldsymbol{r}'|} - e^{-\Lambda_\sigma|\boldsymbol{r}-\boldsymbol{r}'|}). \tag{11a}$$

$$v_\omega(\boldsymbol{r}-\boldsymbol{r}') = \frac{g_\omega^2}{4\pi}\frac{1}{|\boldsymbol{r}-\boldsymbol{r}'|}(e^{-m_\omega|\boldsymbol{r}-\boldsymbol{r}'|} - e^{-\Lambda_\omega|\boldsymbol{r}-\boldsymbol{r}'|}). \tag{11b}$$

where $\Lambda_\sigma = \Lambda_\omega = 1500$ MeV.

In terms of these interactions, we can use the folding method to extend the above-mentioned OP in LDA to the Walecka-model-based RMOP where the lowest-order approximation is considered. Then one can study the effect of the interaction range on the potential. In the Hartree-Fock approximation, both σ- and ω-mesons contribute to the scalar potential V_s, vector potential V_o and three vector potential V_v.

We fold these contributions with the interaction v_l

$$V_i^l(r) = C_l\int V_i^{lLDA}(r)v_l(\boldsymbol{r}-\boldsymbol{r}')\mathrm{d}\boldsymbol{r}', \tag{12}$$

where V^{lLDA} denotes the contribution from the l meson exchange in the mentioned OP in LDA. The resultant real part of the finite nucleus OP reads

$$V_i(r) = V_i^\sigma(r) + V_i^\omega(r). \tag{13}$$

where $i = s$, o, and v. The imaginary part of the potential from polarization diagrams consists three parts. They come from three different processes shown in Fig.1. In the figure, (a) and (b) denote polarization diagrams where σ- and ω-mesons are exchanged twice, respectively, while (c) is the polarization diagram where σ- and ω-mesons are exchanged once, respectively. We symbolize the imaginary potentials from these three diagrams by W^σ, W_ω, and $W^{\sigma\omega}$, respectively. For W^σ and W^ω, we fold OP in LDA twice with corresponding v_l, while for $W^{\sigma\omega}$, we fold OP in LDA with v_σ and v_ω once, respectively. That is

$$W_i^\sigma(r) = C_\sigma^2\int\mathrm{d}\boldsymbol{r}''v_\sigma(\boldsymbol{r}-\boldsymbol{r}'')\int\mathrm{d}\boldsymbol{r}'W_i^{\sigma LDA}(r')v_\sigma(\boldsymbol{r}''-\boldsymbol{r}'), \tag{14a}$$

$$W_i^{\omega}(r) = C_{\omega}^2 \int d\boldsymbol{r}'' v_{\omega}(\boldsymbol{r} - \boldsymbol{r}'') \int d\boldsymbol{r}' W_i^{\omega LDA}(r') v_{\omega}(\boldsymbol{r}'' - \boldsymbol{r})', \tag{14b}$$

and

$$W_i^{\sigma\omega}(r) = C_{\sigma} C_{\omega} \int d\boldsymbol{r}'' v_{\sigma}(\boldsymbol{r} - \boldsymbol{r}'') \int d\boldsymbol{r}' W_i^{\sigma\omega LDA}(r') v_{\omega}(\boldsymbol{r}'' - \boldsymbol{r}'), \tag{14c}$$

The resultant imaginary part of the finite nucleus OP becomes

$$W_i(r) = W_i^{\sigma}(r) + W_i^{\omega}(r) + W_i^{\sigma\omega}(r). \tag{15}$$

In this paper, we use this folding method to improve the calculation of the finite nucleus OP in LDA.

3. NUMERICAL RESULT AND DISCUSSION

In the finite nucleus, the Dirac equation for the nucleon is

$$[(1 + \Sigma_v(r,E))\alpha \cdot \boldsymbol{p} + \gamma^0(M + \Sigma_s(r,E)) - \Sigma_o(r,E)]\Psi = E\Psi. \tag{16}$$

It can be simplified into a form where only scalar and vector potentials are involved.

$$[\alpha \cdot \boldsymbol{p} + \gamma^0(M + U_s) + U_o]\Psi = E\Psi, \tag{17a}$$

where

$$U_s = \frac{\Sigma_s - \Sigma_v M}{1 + \Sigma_v}, U_o = \frac{-\Sigma_o + E\Sigma_v}{1 + \Sigma_v}. \tag{17b}$$

Because, one usually analyze the experimental data in the non-relativistic frame, it is necessary to derive an effective Schrödinger potential. By performing a proper transformation [1,2], one can obtain an equivalent Schrödinger equation

$$[\frac{p^2}{2E} + U_{\text{eff}}(r) + V_c(r) + U_{so}\sigma \cdot L]\varphi(r) = \frac{E^2 - M^2}{2E}\varphi(r), \tag{18}$$

where

$$\varphi(r) = \sqrt{\frac{M + E}{D(r)}}\Psi_>(r),$$

$$D(r) = M + U_s(r) + E - U_o(r) - V_c(r).$$

and $\Psi_>(r)$ is the upper component of the nucleon wave function. The effective Schrödinger central and spin-orbital potentials are

$$U_{\text{eff}}(r) = U_o + \frac{1}{2E}[U_s(2M + U_s) - (U_o - V_c)^2], \tag{19a}$$

and

$$U_{so}(r) = -\frac{1}{2ErD(r)}\frac{dD(r)}{dr}. \tag{19b}$$

Here, we ignore the Darwin term in the central one [7].

In the calculation, we employ the same finite-nucleus density distribution formula given in [1,2], i.e., Negele's empirical formula for heavy nuclei [11] and Gaussian density distribution for light nuclei ^{12}C and ^{14}O [12]. We plot the scalar and vector potentials for P-^{208}Pb at the bombarding energy of 175 MeV. The result shows that at the center area, the calculated OP is almost as same as OP in LDA.

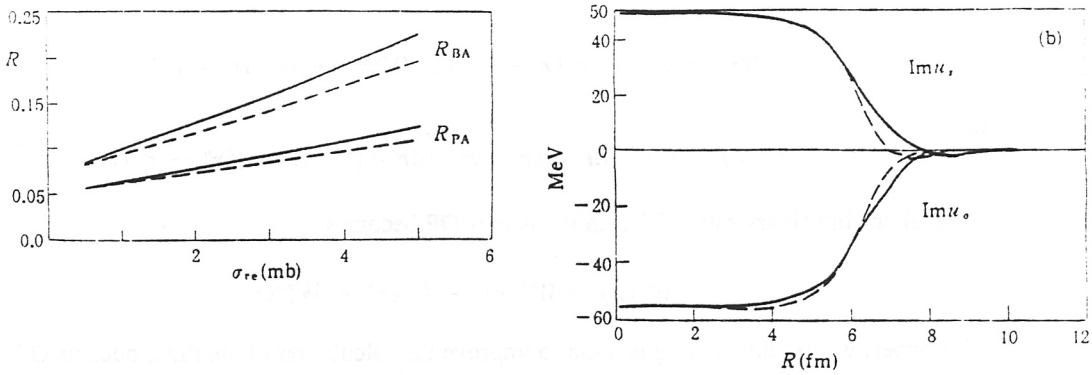

Fig. 2
Scalar and vector potentials for p-^{208}Pb at E = 175 MeV. The solid curve represents our result and the dash curve denotes the result in LDA.

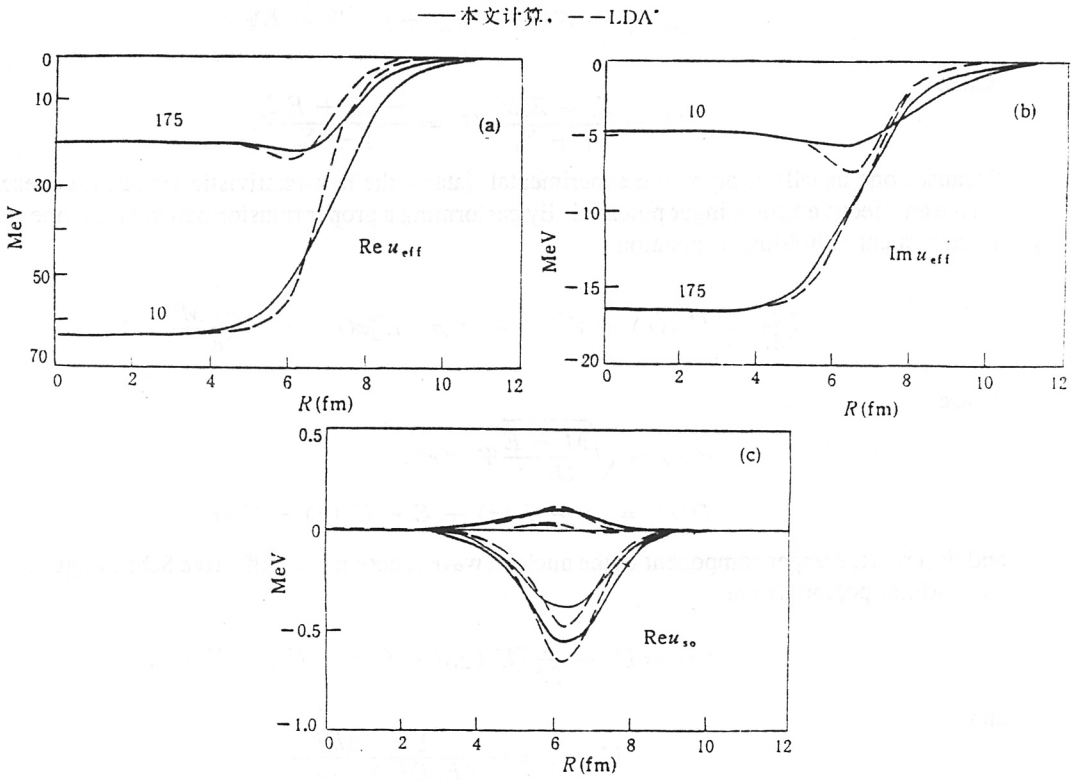

Fig. 3
Effective Schrödinger potential for p-^{208}Pb other notations are the same as those in Fig.2.

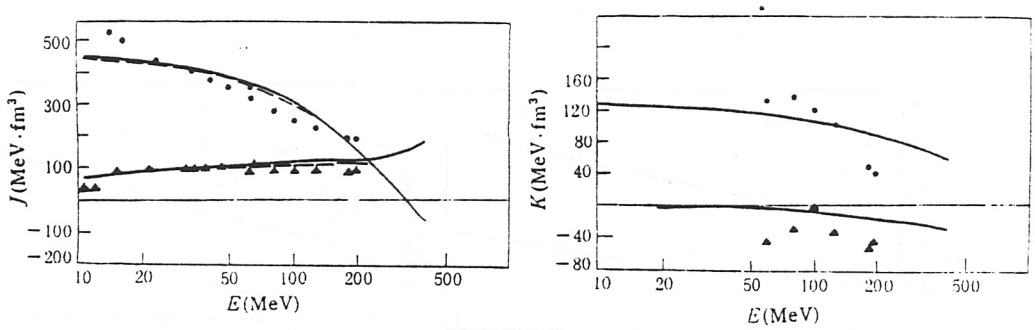

Fig.4

Effective Schrödinger volume integral for p-^{208}Pb. Other notations are the same as those in Fig.2. The experimental data come from [13] and [14].

However, these two potentials are different at the surface region. The former changes more slowly than the latter does with increasing E. Since the interaction range of the nuclear force is rather short, $r_0 \sim 1$ fm, $v_1(\boldsymbol{r} - \boldsymbol{r}')$ goes to zero very fast as $|\boldsymbol{r} - \boldsymbol{r}'| > 1$ fm. Consequently, the folded OP at a certain point only relates to the OP in LDA in a very small region around that point. In the center region of the nucleus, ^{208}Pb OP in LDA is most a constant. After folding, the obtained potential is very close to the original one. In the surface region of the nucleus, the obtained OP in LDA falls down rapidly. After folding, the decreasing tendency of the obtained OP becomes slower. We plot the P-^{208}Pb effective Schrödinger potential at the bombarding energies of 10 MeV and 175 MeV in Fig.3. From this figure, one sees that the change of the central effective Schrödinger potential becomes slow at the surface of the nucleus, the potential apparently moves outward, the depth of the potential at the energy around 175 MeV becomes more shallow, and the spin-orbit potential governed by the differentials of the scalar and vector potentials goes smaller. In comparison with the phenomenological potential, our OP is even closer to phenomenological potential.

Phenomenological analysis indicates that the nucleon-nucleus scattering is very sensitive to the volume integral of the effective Schrödinger potential and the root mean square radius (RMSR). Here, we define the volume integral of the central effective Schrödinger potential as

$$J = -\frac{1}{A}\int u_{\mathrm{eff}}(r)\mathrm{d}\boldsymbol{r}, \tag{20a}$$

the volume integral of the spin-orbital potential as

$$K = -\frac{1}{A^{1/3}}\int u_{so}(r)\mathrm{d}\boldsymbol{r}. \tag{20b}$$

and the RMSR of the real and imaginary parts of the central effective Schrödinger potential as

$$\langle R_{\mathrm{V}}^2\rangle^{\frac{1}{2}} = \left[\frac{\int \mathrm{R_e}(u_{\mathrm{eff}}(r))r^2\mathrm{d}\boldsymbol{r}}{\int \mathrm{R_e}(u_{\mathrm{eff}}(r))\mathrm{d}\boldsymbol{r}}\right]^{\frac{1}{2}}. \tag{21a}$$

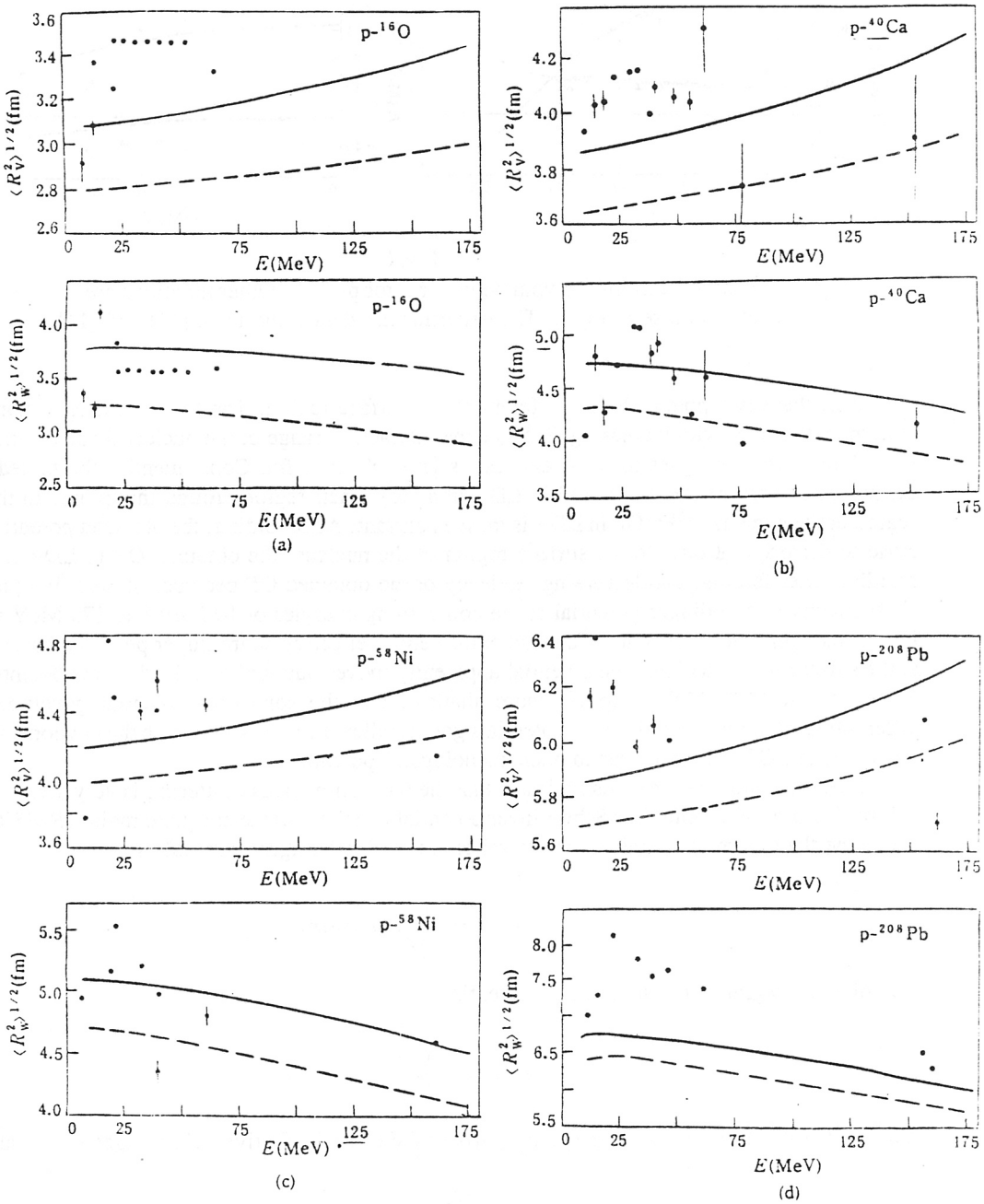

Fig.5

RMSR of the effective central potential. The experimental data come from [13]. Other notations are the same as those in Fig.2.

and

$$R_W^2\rangle^{\frac{1}{2}} = \left[\frac{\int I_m(u_{eff}(r))r^2 dr}{\int I_m(u_{eff}(r))dr}\right]^{\frac{1}{2}}. \tag{21b}$$

respectively.

From Fig.4, one finds that our result does not change the volume integral very much, but do have large effect on the RMSR of the potential. We show the theoretical and phenomenological values of RMSR for p-^{16}O, p-^{40}Ca, p-^{58}Ni and p-^{208}Pb in Fig.5. Apparently, RMSR in LDA is in general smaller than the phenomenological one. In our calculation, RMSR increases and is close to the phenomenological value. This is easily understood from the definition of RMSR. That is, the potential at the large r contributes more to RMSR. In this investigation, the central potential increases in the surface region, consequently, RMSR becomes larger.

To further test the reasonableness of our modified LDA, by using obtained OP, we evaluate the differential cross section of the p-nucleus elastic scattering and related spin observables and compare than with those in LDA. We present the theoretical values and experimental data of the differential cross sections in the p-^{12}C, ^{40}Ca, ^{50}Ni, ^{90}Zr, ^{118}Sn and ^{208}Pb elastic scatterings at the bombarding energy of 65 MeV in Fig.6. Comparing with the values in LDA, our result fits experimental data better. The same conclusion is valid for the differential cross section of the p-^{40}Ca elastic scattering with different bombarding energies shown in Fig.6b. In Fig.7, we give the spin observables, analyzing power $P(\theta)$ and spin rotation function of the p-^{40}Ca and ^{208}Pb elastic scatterings at relevant energies. From this figure, one sees that the improvement for the spin observable is smaller than that for the differential cross section. At $\theta < 40°$, our results fit the experimental data better.

In summary, the potential obtained by folding OP in LDA with the interaction $v_1(\boldsymbol{r}-\boldsymbol{r}')$ is much closer to the phenomenological one. Using this potential to calculate p-^{12}C ~ ^{208}Pb elastic scatterings

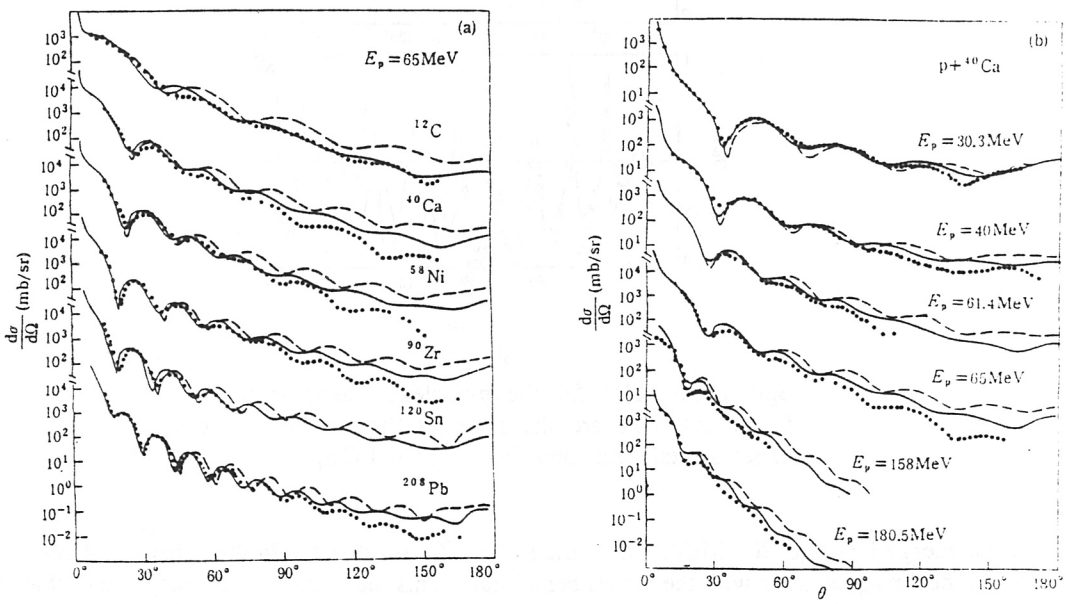

Fig.6

Differential cross sections of the elastic p-nucleus scattering. Other notations are the same as those in Fig.2. The experimental data come from [15] and [16].

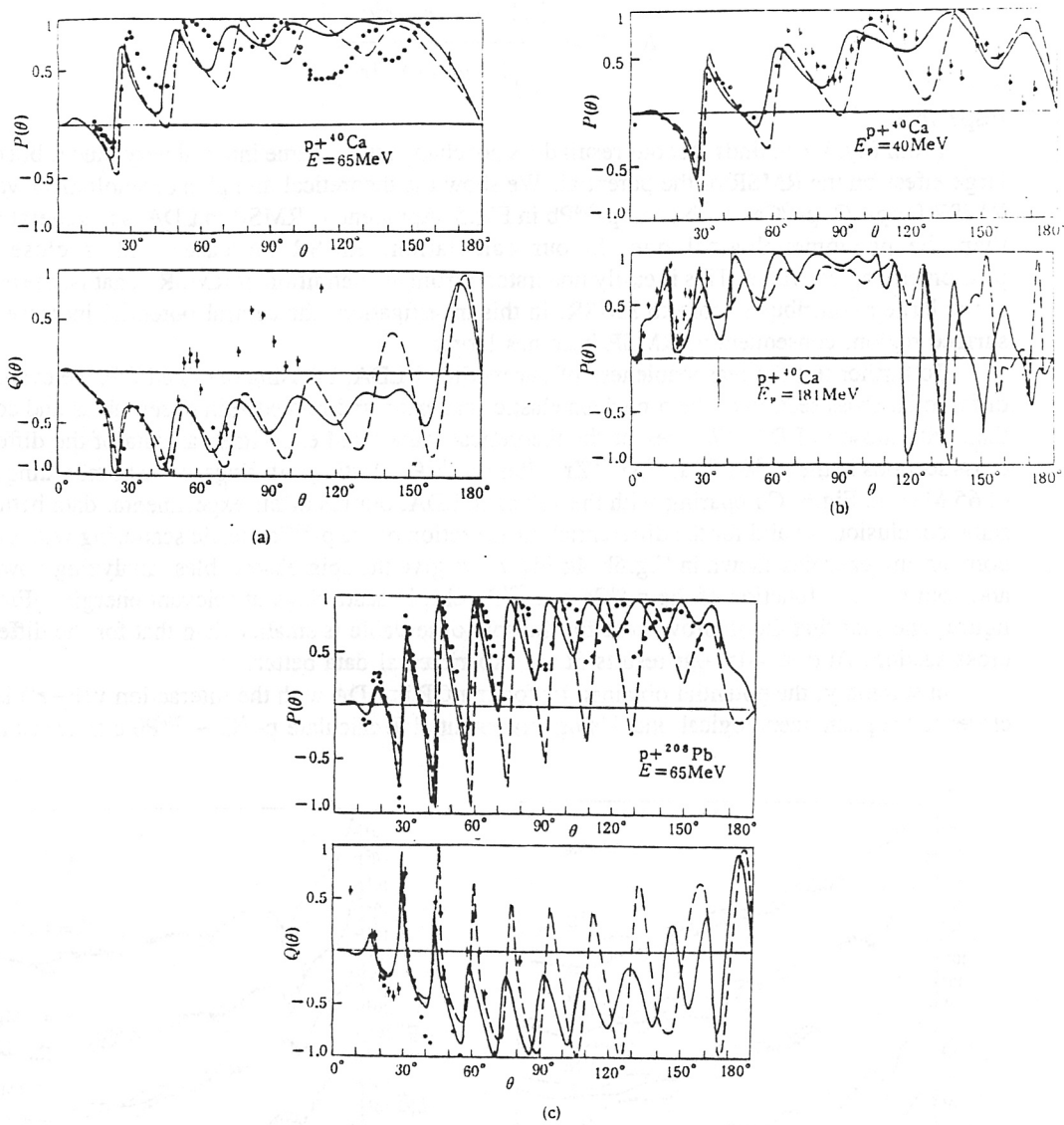

Fig.7

Spin observables for the p-nucleus elastic scattering. Other notations are the same as those in Fig.2. The experimental data come from [15] and [16].

at the energy less than 200 MeV, where the nuclei $^{12}C \sim {}^{208}Pb$ are in the spherical shape, one can obtain better agreements with the experimental data. This indicates that the adoption of this method to consider the effect of the interaction range on the microscopic OP is reasonable. Of course, in this way, we merely take part of this effect into account. Since extending the folding method to the calculations of the Hartree-Fock self-energy and the imaginary self-energy form polarization diagrams as well as the interaction between nucleons are under certain approximations, we only have appreciable

improvement for OP at the surface of the nucleus. On the other hand, the large angle scattering, which relates to the large momentum transfer, depends on the fine structure of the nuclear potential, thus we do not have significant improvement for the large angle scattering.

REFERENCES

[1] Ma Zhongyu et al., *Nucl. Phys.*, **A490**(1988)619.
[2] Zhu Ping et al., *Chinese J. of Nucl. Phys.*, **11**(1989)39.
[3] J.A. McNeil et al., *Phys. Rev. Lett.*, **50**(1983)1439.
[4] C. Nuppena et al., *Nucl. Phys.*, **A571**(1991)525.
[5] L.G. Arnold et al., *Phys. Rev.*, **C23**(1981)1949.
[6] L.G. Arnold et al., *Phys. Rev.*, **C25**(1982)936.
[7] R.C. Clark, Development of the Dirac scattering approach, Invited talk presented at the Los Alamos Workshop on relativistic dynamics and quark-nuclear physics, June 2-14, 1985.
[8] R. Kozack et al., *Nucl. Phys. Rev.*, **C39**(1989)1461.
[9] J.D. Walecka, *Ann. Phys.*, **83**(1974)491.
[10] M. Jaminon, *Phys. Rev.*, **C26**(1982)1151.
[11] J.W. Negele, *Phys. Rev.*, **C1**(1970)1260.
[12] H.F. Ehrenberg et al., *Phys. Rev.*, **113**(1959)666.
[13] J.P. Jeukenne et al., *Phys. Rev.*, **C16**(1977)80.
[14] A. Nadasen et al., *Phys. Rev.*, **C23**(1981)1023.
[15] H. Sakaguchi et al., *Phys. Soc. Jpn. Suppl.*, **55**(1986)61.
[16] B.W. Ridley and J.F. Turner, *Nucl. Phys.*, **58**(1964)497; L.N. Blumberg et al., *Phys. Rev.*, **147**(1966)812; C.B. Folmer et al., *Phys. Rev.*, **181**(1969)1565; A. Johansson et al., *Ark. Fys.*, **19**(1961)541.